PWM LESS CURRENT CONTROL AT VSI-IM DRIVE

Žarko Čučej, Peter Cafuta, and Rajko Svečko
University of Maribor, Slovenia

Keywords: electric motors, IM, Induction Motors, FOC, Field Oriented Control, current control, PWM inverters, Pulse Width Modulated inverters, VSI, Voltage Source Inverters, VSC, Variable Structure Control, BLSC, Boundary Layer Switching Controllers, SCC, Switching Current Control, time-discrete switching variable structure control, optimized mappings

Abstract: This paper discusses time-discrete field oriented variable structure current control of induction motor - voltage source inverter system without use of a pulse-width modulator. The controller is supplemented by feedforward selection of optimized mapping of controllers into voltage source inverter states. This proposed approach of direct inverter control depends on the boundary layer control, and the sign, nominal value and maximal values of the back e.m.f. estimate. It lessens back e.m.f. influence on chattering and makes it possible to extend the field angular velocity range of constant rotor field. Boundary layer control separates variable structure control modes. Supporting preassigned switching order and control objectives is assigned to each attraction domain.

Tokovna regulacija skupka napetostno izvorni pretvornik - izmenični motor brez uporabe modulatorja

Ključne besede: motorji električni, IM motorji indukcijski, FOC krmiljenje v orientaciji polja, krmiljenje tokovno, PWM inverterji modulirani impulzno širinsko, VSI inverterji napetostno izvorni, VSC krmiljenje s strukturo spremenljivo, BLSC, krmilniki komutacijski plasti mejnih, SCC krmiljenje toka komutirajočega, krmiljenje s strukturo spremenljivo časovno-diskretno, preslikave optimirane

Povzetek: Članek obravnava časovno diskretno tokovno regulacijo s spremenljivo strukturo v poljskih koordinatah skupka asinhronski motor - napetostno izvorni pretvornik brez uporabe modulatorja. Regulator je izpopolnjen s predkrmiljenjem izbiranja optimalne preslikave stanj v stanja pretvornika. Ta predlog direktnega krmiljenja pretvornikov je odvisna od režima regulacije in predznaka, minimalne ter maksimalne inducirane napetosti v motorju. Z njo se v veliki meri kompenzira vpliv inducirane napetosti motorja na drhtenje. V primerjavi z običajnimi rešitvami omogoči tudi razširitev vrtne hitrosti pri konstantnem rotorskem polju. Pasovni regulator razmeji režime regulacije s spremenljivo strukturo. Vsakemu režimu predpiše atrakcijsko domeno, ki omogoča predpisano zaporedje preklapljanja in kriterije kvalitete regulacije.

1 Introduction

For an Induction Motor (IM) the Pulse-Width Modulation (PWM) of the Voltage Source Inverter (VSI) plays an important role in the control system, since not only the level but also the phase of input signal must be controlled. These occur as certain disadvantages of PWM inverters because they are determined by the characteristics of PWM and are not addressable by controllers /1/. These drawbacks can be eliminated by switching the variable structure (which has a direct control VSI - IM system) constructed by signals as the position, velocity, and currents, which contain information about disturbances and parameter variation, consequently the entire control system is completely accessible to control and can be optimized in a Variable Structure Control (VSC) design.

Unfortunately, time-discrete implementation of switching type VSC causes chattering, degrading all the benefits of direct switching control. In /2/,/3/ we describe chattering reduction using hysteresis controllers and in /4/ using finite automaton. The recent article /5/ proposes quasi VSC implemented with a first order deadbeat controller and a space-vector PWM. Regardless of the fact that the obtained average current error is smaller than at direct switching control, this solution has some serious limitations. Disturbances should be smooth and limited, control robustness depends on the disturbance estimator used, and PWM properties are uncontrollable.

In this paper we present the Boundary Layer Switching Controller (BLSC) used in Field Oriented Control (FOC) adapted with a feedforward steering selection for mapping of the controllers states into VSI states. Using BLSC the fixed order switching is determined, and to each of its phases mapping is optimized in regard to the following control objectives:

- sliding mode reaching time,
- average current error offset,
- chattering,
- VSI switching losses.

Mapping optimization compared to /6/ involves zero voltage vectors. This introduced feedforward selection is similar to predictive current control /7/, except that: (i) the control is still VSC, and (ii) instead of back e.m.f., only information about the field velocity sign, and minimal and maximal values of back e.m.f. estimates are used.

This work was supported in part by the Slovene Research Ministry under Grant J2-1644-0796-99.

This article is organized as follows. Problem presentation with description of VSI, IM model and a summary of VSC is contained in section 2. In section 3 the proposed control with compensation of back e.m.f., feedforward steering and design of ST is given. Results of simulations are collected in section 4. This article ends with conclusions and appendices containing derivation of zero dynamics, IM model and analysis of stability for use of zero voltages.

2. Problem presentation

IM is feed by a 3-leg bridge VSI supplied by DC voltage *E* and direct controlled by current switching controllers in the inner loop of FOC. VSI has eight states, which determine six active voltage vectors $\boldsymbol{u}_k, k = 1,\ldots 6$ with constant amplitude $u_k = 2E/3$ and two zero voltage vectors $\boldsymbol{u}_k \in \{\boldsymbol{u}_0, \boldsymbol{u}_7\}$ (Fig. 1).

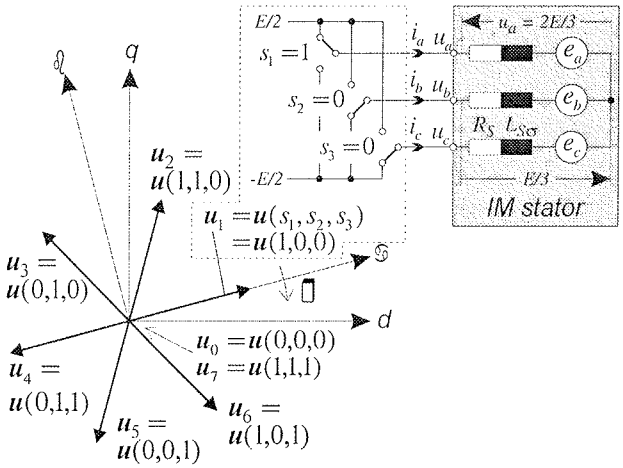

Fig. 1: Voltage vector representation from the d-q frame perspective, inverter, and load circuit.

A symmetrical, 3-phase IM with Y stator windings with a galvanic isolated central tap is considered. Its voltage model in *d-q* frame is described by the following MIMO system:

$$u_\Diamond = Ri_S + L_{S\sigma} p i_{S\Diamond} + e_\Diamond \,, \Diamond \in \{d, q\}, \qquad (1)$$

where $\boldsymbol{u} = [d\ q]^T$ is stator voltage vector, R_S and $L_{S\Diamond}$ are rotor resistance and rotor leakage inductance respectively, $e_\Diamond$ is sum of back e.m.f. and crosscoupled voltages ($e_d = e_{dq} + e_{di}$, $e_q = e_{qd} + e_{qi}$), and $pi = di/dt$. Latter, in the design we use a simple modified model:

$$L_{S\sigma} p i_{S\Diamond} = u_{k\Diamond} - e_\Diamond \,, \qquad (2)$$

which is derived in Appendix C.

2.1 FOC

We assumed that FOC has a multi-loop structure and is sampled every T_S seconds, i.e. algorithms are implementable in the digital signal processor. Outer loops contain state controllers and estimators for the load torque T_L, rotor magnetization current i_{mR}, and angle ϑ. They are responsible for the tracking of drive kinematics variables and the regulation of i_{mR}. Field weakening is not considered. The selection of design coefficients c_1, c_2, and c_3 (elaborated in Appendix A and Appendix B) of outer control loops should guarantee stable *zero dynamics* with a stationary point: $\tilde{\varphi} = \dot{\tilde{\varphi}} = \psi_R = 0$ and $\dot{\tilde{\varphi}} = \ddot{\tilde{\varphi}} = \dot{\psi}_R = 0$. Outputs from outer loops i_{Sq}^{REF} and i_{Sd}^{REF} serve as command values for inner current control loops.

2.2 Current variable structure control

The control problem being considered is a determination of sequence and the duration of VSI states, so that by tracking i_{Sq}^{REF} and i_{Sd}^{REF} the drive FOC is satisfied:

$$\boldsymbol{s} = \left[s_d\ s_q\right]^T = \boldsymbol{i}_S^{REF} - \boldsymbol{i}_S = 0 \,, \qquad (3)$$

i.e. VSC is established in stator currents error space $\square^2$ where $s_\Diamond = 0$, $\Diamond \in d, q$ are switching subspaces. This formulation embraces the control of stator currents and modulation of VSI outputs as one problem, which is solved by a MIMO VSC.

It is well known /9/, /10/, that the design of VSC can be done by satisfying a reaching condition. In FOC the torque and magnetization control are decoupled, meaning that the MIMO current control is designed by two independent controllers, which fulfill reaching conditions written in compact form as:

$$S_D : \dot{s}_d s_d < 0 \qquad (4a)$$

$$S_Q : \dot{s}_q s_q < 0 \qquad (4b)$$

$$S_0 : S_D \cap S_Q \qquad (4c)$$

by discontinuous control:

$$v_\Diamond = \begin{cases} v_\Diamond^- & \text{if } s_\Diamond > 0 \\ v_\Diamond^+ & \text{if } s_\Diamond < 0 \end{cases} \qquad (5)$$

with discontinuity on the switching subspaces S_i. The set of control vectors $\boldsymbol{v} = \left[v_d\ v_q\right]^T \in \boldsymbol{v}_j$, $j = 1,\ldots 4$ is present-

ed in Fig. 2a. Control (5) ensuring (in ideal circumstances, when switching frequency is infinite) or sliding on S_D with reaching to S_0, or sliding on S_Q with reaching to S_D either sliding on S_0. Only in the last case is the request (1) completely satisfied.

The PWM's less mapping between control vector ***v*** and stator voltage vector ***u*** gives IM stator voltage equation (2). Combining (4a), (4b) and (1) gives:

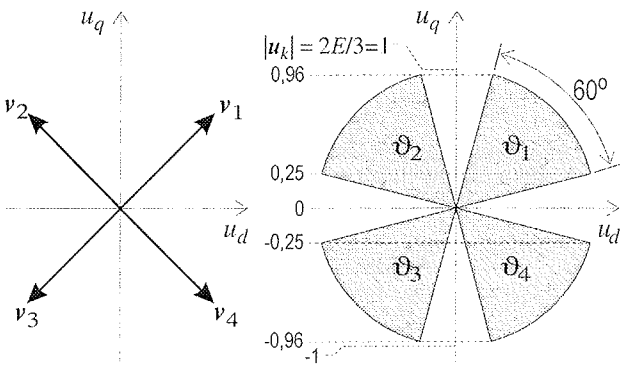

Fig 2: Presentation of control vectors (a) and mapping range (b).

$$\left[\frac{1}{L_{S\sigma}}\left(u_{k\Diamond}-e_{\Diamond}\right)\right]s_{\Diamond}<0\rightarrow\begin{matrix}s_{\Diamond}<0\,,\,u_{k\Diamond}>e_{\Diamond}\\ s_{\Diamond}>0\,,\,u_{k\Diamond}<e_{\Diamond}\end{matrix}\qquad(6)$$

If VSC, for control robustness is designed at $\max|e_{\Diamond}|$, for mapping $v\rightarrow u$ from (6) it follows:

$$v_{\Diamond}=u_{k\Diamond}(\rho)=\begin{cases}v_{\Diamond}^{-} & \text{when}\quad u_{k\Diamond}<-\max|e_{\Diamond}|\\ v_{\Diamond}^{+} & \text{when}\quad u_{k\Diamond}>\max|e_{\Diamond}|\end{cases}\qquad(7)$$

Due to the rotation of the active voltage vectors and their angular displacement at 60^0, the mapping $v\rightarrow u$ links control vectors $\{v_j\}$ with four angular sectors $\{\vartheta_j\}$ in *d-q* frame containing voltage vectors $\{u_k\}$ involved in mapping.

The sectors placements depend on terms $e_{\Diamond}$ (or $d_{\Diamond}$, see (31) in Appendix C), but in the case of (7) only on their maximal amplitude. Therefore angle sectors are placed symmetrically as are the symmetrical control vectors v_j (Fig. 2b).

2.3 Implementation of decoupled switching current control

This described current control is named decoupled Switching Current Control (SCC). It is of simple structure (Fig. 3) and can be simply implemented using digital signal processors. ST performs mapping where selection of columns addressed by ρ quantizer performs an inverse transformation from *d-q* to *abc* space.

Time discrete implementation of the decoupled SCC causes inverter outputs to have a finite pulse such as pulse width modulation. Their duration is equal to one sample interval and occasionally to an integer multiple of T_s. Therefore the decoupled SCC is never in SM. Consequently difference in control vector amplitudes, i.e. $|\overline{v_{\Diamond}^{-}}|-|\overline{v_{\Diamond}^{+}}|=|\overline{e_{\Diamond}}|$ cause offset in $|\overline{e_{\Diamond}}|$ and subharmonic oscillation (in regard to frequency $1/T_s$) of local average of $|\overline{e_{\Diamond}}|$ (determined by stator time constant) causing torque chattering.

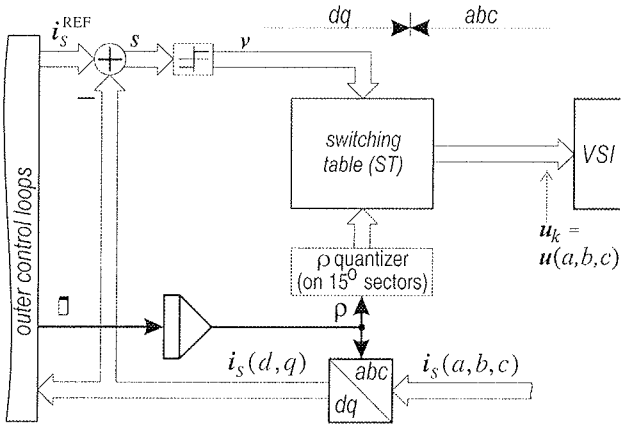

Fig. 3: Realization of decoupled SCC.

The other important drawbacks of mapping (7) are: (i) zero vector voltages are uninvolved, and (ii) for components of the selected voltage vector the following holds

$$\max|u_d|=\max|u_q|\quad\text{and}\quad\min|u_d|=\min|u_q|,\qquad(8)$$

which limits the velocity range of nominal magnetization to:

$$\max e_{\Diamond}\le 0{,}25\left(2E/3\right)\qquad(9)$$

Absence of zero voltages cause high total switching frequency of VSI (at least twice that of $1/T_s$), consequently VSI switching losses are very high.

3 Proposed switching current control

Decoupled SCC performances are well enhanced with Fixed-order sliding mode switching scheme /10/, where the sliding mode takes its place in a preassigned order while state is traversing the state space:

- moving along S_D only in initialization phase during the establishment of nominal rotor magnetization;
- in regular control it mode moves in order

$$S_Q \rightarrow S_0 \tag{10}$$

and then maintaining limit cycle around S_0. Mappings supporting (10), should adopt attraction to VSC modes. For S_Q the minimal S_0 reaching time is requested, after reaching S_0 it is desirable to maintain the limit cycle around ***s***-origin so, that the current ripple is redirected from torque into magnetization control (where it is well dumped by large rotor lag) and in VSI switching sequences the minimal number of switches is involved. This is achieved by deliberate use of zero voltage vectors in mapping.

3.1 Boundary Layer Switching Control

The fixed-order sliding mode switching scheme is made possible by the Boundary Layer Switching Control (BLSC), which separates the associated VSC modes. According to above description it has to differentiate between three VSC modes:

- mode of moving along S_Q
- mode of limit cycle at S_0, which has two phases:
  - phase of obeying (4b).
  - phase of obeying (4c).

These modes besides the mapping range presented in Fig. 2b, which accommodates attraction domain A_{DQ}, need two further domains:

- domain A_0 belonging S_0, where v_q^-, v_d^+ are mapped into ***u*** with minimal amplitudes of u_{kq} fulfilling (6), and v_d^-, v_d^+ into ***u*** with maximal amplitudes of u_{kq},
- domain A_Q belonging S_Q where mapping requests are opposite to requests for domain A_0.

BLSC, which fulfills the above requirements, has three layers of coaxial arrangement with a center in ***s***-plane origin (Fig. 4).

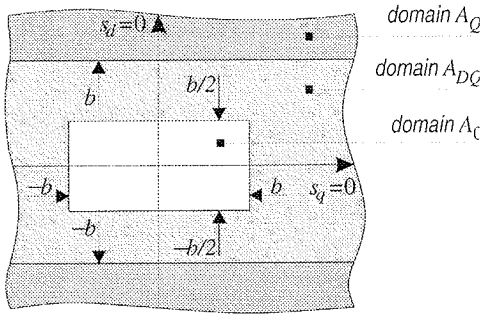

Fig. 4: Borders and discrete VSC modes.

The borders between attraction domains are determined by the current error caused by maximal voltage amplitude, which arises in a stationary condition in one sampling interval. Using the estimation of $\dot{s}_q$ with difference $\Delta s_q / T_s$ for border between A_Q and A_{DQ} we can state:

$$|b| = \frac{\|u\|}{L_{S\sigma}} T_s . \tag{11}$$

For inner border (between A_{DQ} and A_0) we consider in (11) maximal allowed back e.m.f.. Because

$$\frac{\|u\|}{\max|e_q|} \geq 2 \tag{12}$$

it follows, that in *q* direction the inner border is $b/2$. Boundaries in *d* direction we settled to $\pm b$. This choice is based on a consideration that in the limit cycle around the error plane origin ($s = 0$) a sequence of voltage vectors could be formed, where zero voltage vectors follow each active vector. In this case the border in *d* direction should be at least so far from the origin of ***s***-plane that s_d, i.e. current error in *d* direction can be zeroed by $\max|u_d|$. Thus borders in *d* direction should be calculated similarly to borders in *q* direction, i.e. by (11) with consideration for adequate voltages in *d* direction. Because $\max|u_d| = \max|u_q|$ and $\max|e_d| \leq \max|e_q|$ we justify aforementioned choice of $\pm b$ for *d* direction.

Note, the boundaries are tied to the sampling interval T_S, and their size actually determines the duration of sampling interval. In many IM control designs, the value of the sampling interval T_S is influenced more by desired rotor field angular accuracy, the rms value of stator current chattering, and inverter volume power density than by IM dynamic requests. One of this project's goals was to make the sampling interval as short as possible in regard to the limitations of the used digital signal processor. The target value was 25 μs.

3.2 Compensation of e_q

Use of zero voltage vectors u_0, u_7 in mapping during limit cycle reduces offset and chatter of $s_\Diamond$ local average (in interval determined by the motor's time constants respectively), but for dump these phenomena, $e_\Diamond$ should be compensated.

Due to switching controllers they cannot be compensated by subtraction of $e_\Diamond$ as is done for predictive controllers /

/7/. Rather, the slowly-occurring magnetization offset (caused by e_d) is minimized by rotor magnetization control (see Appendix B), and oscillation of local average of s_q causing torque chattering, is effectively minimized by mapping with property

$$\overline{|v_q^+|} = \overline{|v_q^-|} \,. \tag{13}$$

From (7) at $e_q > 0$ follows $v_q^- = u_q^- + e_q$ and $v_q^+ = u_q^- - e_q$ where u_q^-, u_q^+ denotes voltages to which v_q^- and v_q^+ are mapped, consequently the above equation can only be fulfilled if at least the sign, min and max of e_q is known. By rough linearization of $u_q = \|\boldsymbol{u}\| \sin\rho$, considering $e_q > 0$ and limit $\min\left(v_q^+\right) = \max\left(e_q\right)$, after a short calculation we obtain:

$$\min\left|u_q^-\right| = -\min\left|e_q\right| \,. \tag{14}$$

This suboptimal solution enables a simple construction of the angular sectors distributions. Moreover, exact calculation in the case of $\min\left(e_q\right)$ is by (7) limited to (14).

Mapping, considering (13) and (14) and the preassigned switching order is then:

$$u_{kd}(\rho) - e_d \rightarrow \begin{cases} v_d^- & \text{when} \quad s_d > 0 \\ v_d^+ & \text{when} \quad s_d < 0 \end{cases} \tag{15a}$$

$$u_{kq}(\rho) - e_q \rightarrow \begin{cases} v_q^- & \text{when} \quad u_{kq} > -\min\left|e_q\right| \\ v_q^+ & \text{when} \quad u_{kq} < \max\left|e_q\right| \end{cases} \tag{15b}$$

$$u_{kq}(\rho) + e_q \rightarrow \begin{cases} v_q^- & \text{when} \quad u_{kq} < \min\left|e_q\right| \\ v_q^+ & \text{when} \quad u_{kq} > -\max\left|e_q\right| \end{cases} \tag{15c}$$

where (15b) and (15c) are valid for positive and negative e_q respectively.

The position of angular sectors θ_j, containing vectors $\boldsymbol{u}_k$ is determined by the geometric relationship between $|u_q|$ and $|\boldsymbol{u}(\rho)|$ at ρ_{jB} and ρ_{jE}, where angles ρ_{jB} and ρ_{jE} denote the beginning and end of angular sector ϑ_j (Fig.5). At $\rho > 0$ for odd sectors ρ_{1B} and ρ_{1E} can be generally written as:

$$\sin\rho_{1B} \geq \frac{\min e_q}{\|\boldsymbol{u}\|} \quad , \quad \sin\rho_{3B} \geq \frac{\min e_q}{\|\boldsymbol{u}\|} \,. \tag{16}$$

Sector ϑ_1 is placed in $\rho_{1B} \leq \rho \leq \rho_{1B} + \frac{\pi}{3}$ and similarly for sector ϑ_3 hold $\rho_{3B} \leq \rho \leq \rho_{3B} + \frac{\pi}{3}$. When hold $\dot{\rho} < 0$, then we obtain:

$$\sin\rho_{1B} \geq \frac{\min e_q}{\|\boldsymbol{u}\|} \quad , \quad \sin\rho_{3B} \leq \frac{\min e_q}{\|\boldsymbol{u}\|} \,. \tag{17}$$

The position of even sectors ϑ_2 and ϑ_4 are symmetrically over q-axe to position of ϑ_1 and ϑ_2 respectively.

Zero voltage vectors take place in A_0 domain only and their selections is independent of field angle ρ. They are applied according to:

$$\begin{aligned} &\texttt{if } \boldsymbol{u}\left[(n-1)\mathrm{T_s}\right] = \boldsymbol{u}_7 \vee \boldsymbol{u}_2 \vee \boldsymbol{u}_4 \vee \boldsymbol{u}_6 \\ &\quad \texttt{then } \boldsymbol{u}\left(n\mathrm{T_s}\right) = \boldsymbol{u}_7 \\ &\quad \texttt{else } \boldsymbol{u}\left(n\mathrm{T_s}\right) = \boldsymbol{u}_0 \end{aligned} \tag{18}$$

where nT_S is the sampling instant. This selection gives minimal VSI over-switching at the voltage vectors change [2]. As this is excellent for VSI and enables good compensation of e_q, it should be noted that at zero vector voltage the IM is effectively allowed to coast. Control seems to be lost during this time, but stability is still preserved because besides conditions (33) and (10) the following condition

$$\operatorname{sign} s_q = \operatorname{sign} e_q \tag{19}$$

is also fulfilled (see stability analysis in Appendix D).

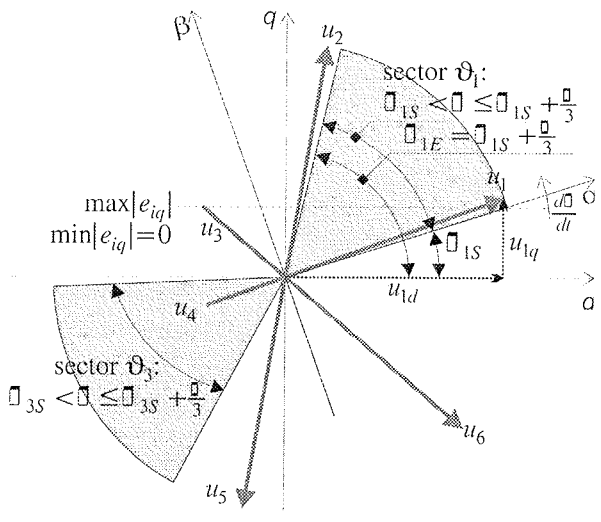

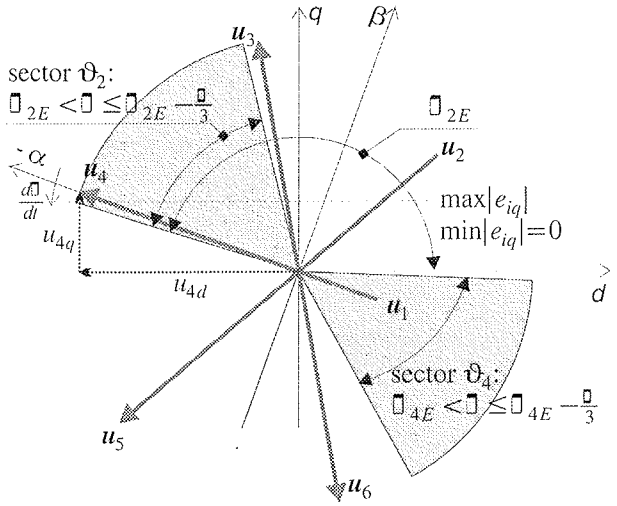

Fig. 5: Determination of ρ_{jB} and ρ_{jE} in nominal field angular velocity range.

3.3 Implementation of proposed current control

The structure of the proposed current switching control is shown in Fig. 6. BLSC is implemented by a 2-dimensional 4-level quantizer separating the attractors domains A_0, A_{DQ} and A_Q. Switching table ST is result of logic superposition of angular sectors determined in subsections 3.1 and 3.2 respectively. Feedforwarded $\dot{\rho}$ is quantized by a four-level quantizer. It determines max and min value of back e.m.f. (because $e_q = e_{iq} + e_{dq}$, whereas constant field is proportional to $\dot{\rho}$ and e_{dq} varies according to $\dot{\rho}$ and fast i_{Sd}, it is simple to evaluate $\max e_q$ and $\min e_q$ for positive and negative angular velocity range of $\dot{\rho}$). In the case, where distinguishing between A_{DQ} and A_Q domains is less important than maximal $\dot{\rho}$ with constant rotor field, the voltage range for A_Q can be exploited in A_{DQ} domain. This in comparison to decoupled SCC enables to doubling of the $\dot{\rho}$ range of the constant rotor field, Table 1.

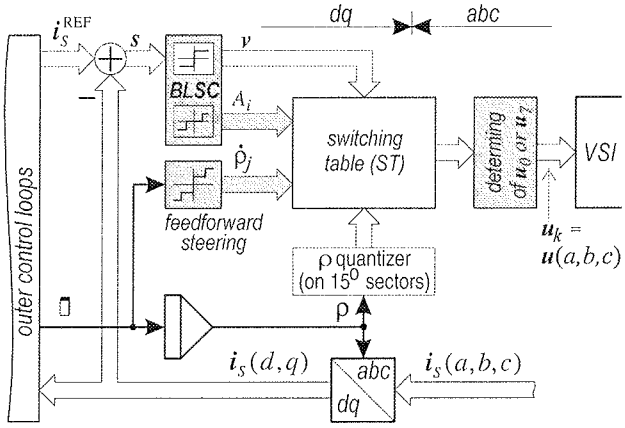

Fig. 6: Proposed control with mapping and feedforward steering.

Table 1: Pairs $\max e_q$ - $\min e_q$ in nominal and extended velocity ranges. $\dot{\rho}_{SCC}$ is maximal $\dot{\rho}$ range of SCC.

velocity range	$\max e_q$	$\min e_q$
$\dot{\rho}_{SCC} \geq \rho \geq 0$	0,25(2E/3)	0
$0 \geq \rho \geq -\dot{\rho}_{SCC}$	0	– 0,25(2E/3)
$2\dot{\rho}_{SCC} \geq \rho \geq \dot{\rho}_{SCC}$	0,5(2E/3)	0,25(2E/3)
$-\dot{\rho}_{SCC} \geq \rho \geq -2\dot{\rho}_{SCC}$	-0,25(2E/3)	– 0,5(2E/3)

ST consists of 9 subtables, see Table 2. They are addressed by attractors domains A_i and angular velocity range ρ_j. The rows in the subtable are determined by the signum functions of BLSC. Columns are addressed by ρ quantizer determining 24 angular quants θ_c. The inverse transformation from *d-q* to *abc* frame is the domain of columns. Determination of zero voltage vectors according to (18) follows ST.

Table 2: Switching table (ST). The VSI switches states are denoted by the corresponding voltage vectors.

	θ_1 : $0 \geq \rho \geq -\frac{\pi}{12}$											
v	$\cdots$	$\theta_{2'}$	θ_1	θ_2	θ_3	θ_4	θ_5	θ_6	θ_7	θ_8	θ_9	$\cdots$
	subtable #1: A_{DQ} ; $\dot{\rho}_{SCC} > \dot{\rho} > -\dot{\rho}_{SCC}$											
v_1	$\cdots$	u_5	u_5	u_5	u_5	u_6	u_6	u_6	u_6	u_1	u_1	$\cdots$
v_2	$\cdots$	u_6	u_6	u_1	u_1	u_1	u_1	u_2	u_2	u_2	u_2	$\cdots$
v_3	$\cdots$	u_2	u_2	u_2	u_2	u_3	u_3	u_3	u_3	u_4	u_4	$\cdots$
v_4	$\cdots$	u_3	u_3	u_4	u_4	u_4	u_4	u_5	u_5	u_5	u_5	$\cdots$
	subtable #2: A_Q ; $\dot{\rho}_{SCC} > \dot{\rho} > 0$											
v_1	$\cdots$	u_3	u_4	u_4	u_4	u_4	u_5	u_5	u_5	u_5	u_6	$\cdots$
v_2	$\cdots$	u_6	u_1	u_1	u_1	u_1	u_2	u_2	u_2	u_2	u_3	$\cdots$
v_3	$\cdots$	u_2	u_2	u_2	u_3	u_3	u_3	u_3	u_4	u_4	u_4	$\cdots$
v_4	$\cdots$	u_3	u_3	u_3	u_4	u_4	u_4	u_4	u_5	u_5	u_5	$\cdots$
	subtable #3: A_Q ; $0 > \dot{\rho} > -\dot{\rho}_{SCC}$											
v_1	$\cdots$	u_5	u_5	u_5	u_6	u_6	u_6	u_6	u_1	u_1	u_1	$\cdots$
v_2	$\cdots$	u_6	u_6	u_6	u_1	u_1	u_1	u_1	u_2	u_2	u_2	$\cdots$
v_3	$\cdots$	u_1	u_2	u_2	u_2	u_2	u_3	u_3	u_3	u_3	u_4	$\cdots$
v_4	$\cdots$	u_3	u_4	u_4	u_4	u_4	u_5	u_5	u_5	u_5	u_6	$\cdots$
	subtable #4: A_0 ; $\dot{\rho}_{SCC} > \dot{\rho} > 0$											
v_1	$\cdots$	u_5	u_5	u_5	u_6	u_6	u_6	u_6	u_1	u_1	u_1	$\cdots$
v_2	$\cdots$	u_6	u_6	u_6	u_1	u_1	u_1	u_1	u_2	u_2	u_2	$\cdots$
v_3, v_4	zero voltage vectors, determined by (18)											
	subtable #5: A_0 ; $0 > \dot{\rho} > -\dot{\rho}_{SCC}$											
v_1, v_2	zero voltage vectors, determined by (18)											
v_3	$\cdots$	u_1	u_2	u_2	u_2	u_2	u_3	u_3	u_3	u_3	u_4	$\cdots$
v_4	$\cdots$	u_3	u_4	u_4	u_4	u_4	u_5	u_5	u_5	u_5	u_6	$\cdots$
	subtable #6: A_{DQ} , A_Q ; $\dot{\rho} > \dot{\rho}_{SCC}$											
v_1	$\cdots$	u_3	u_4	u_4	u_4	u_4	u_5	u_5	u_5	u_5	u_6	$\cdots$
v_2	$\cdots$	u_6	u_1	u_1	u_1	u_1	u_2	u_2	u_2	u_2	u_3	$\cdots$
v_3	$\cdots$	u_2	u_2	u_2	u_3	u_3	u_3	u_3	u_4	u_4	u_4	$\cdots$
v_4	$\cdots$	u_3	u_3	u_3	u_4	u_4	u_4	u_4	u_5	u_5	u_5	$\cdots$
	subtable #7: A_{DQ} , A_Q ; $-\dot{\rho}_{SCC} > \dot{\rho}$											
v_1	$\cdots$	u_5	u_5	u_5	u_6	u_6	u_6	u_6	u_1	u_1	u_1	$\cdots$
v_2	$\cdots$	u_6	u_6	u_6	u_1	u_1	u_1	u_1	u_2	u_2	u_2	$\cdots$
v_3	$\cdots$	u_1	u_2	u_2	u_2	u_2	u_3	u_3	u_3	u_3	u_4	$\cdots$
v_4	$\cdots$	u_3	u_4	u_4	u_4	u_4	u_5	u_5	u_5	u_5	u_6	$\cdots$
	subtable #8: A_0 ; $\dot{\rho} > \dot{\rho}_{SCC}$											
v_1	$\cdots$	u_3	u_4	u_4	u_4	u_4	u_5	u_5	u_5	u_5	u_6	$\cdots$
v_2	$\cdots$	u_6	u_1	u_1	u_1	u_1	u_2	u_2	u_2	u_2	u_3	$\cdots$
v_3, v_4	zero voltage vectors, determined by (18)											
	subtable #9: A_0 ; $-\dot{\rho}_{SCC} > \dot{\rho}$											
v_1, v_2	zero voltage vectors, determined by (18)											
v_3	$\cdots$	u_1	u_2	u_2	u_2	u_2	u_3	u_3	u_3	u_3	u_4	$\cdots$
v_4	$\cdots$	u_3	u_4	u_4	u_4	u_4	u_5	u_5	u_5	u_5	u_6	$\cdots$

4. Simulation

A property of the proposed control with feedforward steering of optimized mappings has been evaluated by simulation. Data for IM, VSI, controllers, and perturbed tracking task considered in simulations are collected in Table 3.

Table 3: Motor, inverter, controllers, and task data.

Motor:	four pole, 1480 rpm, Y connected stator windings with isolated central tap		
Parameters:	$R_S = 0,65\,\Omega$	$L_S = 1,65$ mH	$T_e = 4$ Nm
	$\tau_R = 0,12$ s	$J = 0,000656$ kgm^2	
Inverter:	3-phase bridge, supply voltage $E = 310$		
Control:		SCC	proposed
	BLSC border: b	-	3 A
	magnetization reference i_{mR}^{REF}	4,75 A	4,75 A
Kinematics:	$c_1 = 70000$, $c_2 = 1000$, $c_3 = 100$		
Perturbed tracking task:	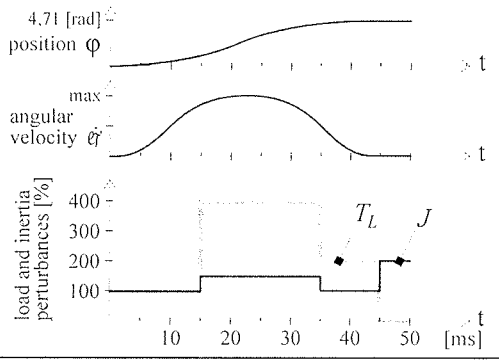		

The chosen task enables testing of the proposed mapping in all VSC modes. Simulation starts by initialization, where the nominal rotor magnetic field is established, then A_Q and A_{DQ} follow, which are disturbed in 15^{th} milliseconds with a change of the load torque. It pushes VSC into RM. The perturbation of the inertia J is used for evaluation of the robustness against IM parameter variation.

To show the properties of the proposed mapping, a comparison to SCC (characterized by Fig. 2b and presented in Fig. 3) has been made. The significant simulation results are collected in Table 4, and shown in Fig. 7.

From these results it follows that the proposed mapping with optimized voltage patterns has several advantages in comparison to SCC:

- the number of switches involved in voltage vector switch-over and the number of voltage vector changes are reduced by 60 % and 40 % respectively,
- chattering of i_{sq} is reduced by 40 %,
- reduction of $(i_S)_{rms}$ 1,73 % slightly reduces motor losses,
- the angular velocity range of the constant rotor field is doubled,
- tracking of kinematics variable is slightly improved.

Table 4: Simulation results.

parameter		SCC	proposed
$\max(i_{Sq}) - \min(i_{Sq})$	[A]	20,26	10,83
$\overline{i_{Sq}}$	[A]	12,51	12,62
$(i_{Sq})_{rms}$	[A]	13,39	12,97
$\overline{\max(i_{Sq}) - \min(i_{Sq})}\Big/\overline{i_{Sq}}$		1,62	0,87
$\max(i_{Sd}) - \min(i_{Sd})$	[A]	4,92	5,96
$\overline{i_{Sq}}$	[A]	0,93	0,57
$(i_{Sq})_{rms}$	[A]	1,98	2,17
$(i_S)_{rms}$	[A]	13,39	13,15
u changes frequency	[Hz]	19800	11400
total switch-over freq.	[Hz]	48200	18800
end position error $\Delta\varphi$	[rad]	-0,087	-0,066

The complexity of the algorithms and the target sampling interval was tested by implementation of algorithms on the floating point digital signal processor AT\&T C32 using a 40 MHz clock. The following results were achieved:

- the boundary layer controller with feedforward steering needs about 4 μs, and
- the measurement of i_{Sd} and i_{Sq}, and the calculation of ρ need about 14 μs.

From the above it can be concluded that the sampling interval of $T_s = 25\,\mu s$ at IM servo-drive system with proposed current control can be easily achieved.

5. Conclusion

The presented PWM less switched field oriented control with feedforward selection of subtable with optimized mapping has been investigated analytically and evaluated by simulations. The obtained results show that the proposed switching current control significantly reduces the drawbacks of decoupled SCC, i.e. chattering, offsets and inverter switching losses. The achieved improvements are based on the deliberate use of the reaching condition resulting in of preassigned switching order, time scale sepa-

reference solution:
de-coupled SCC
from Fig. 3

proposed solution

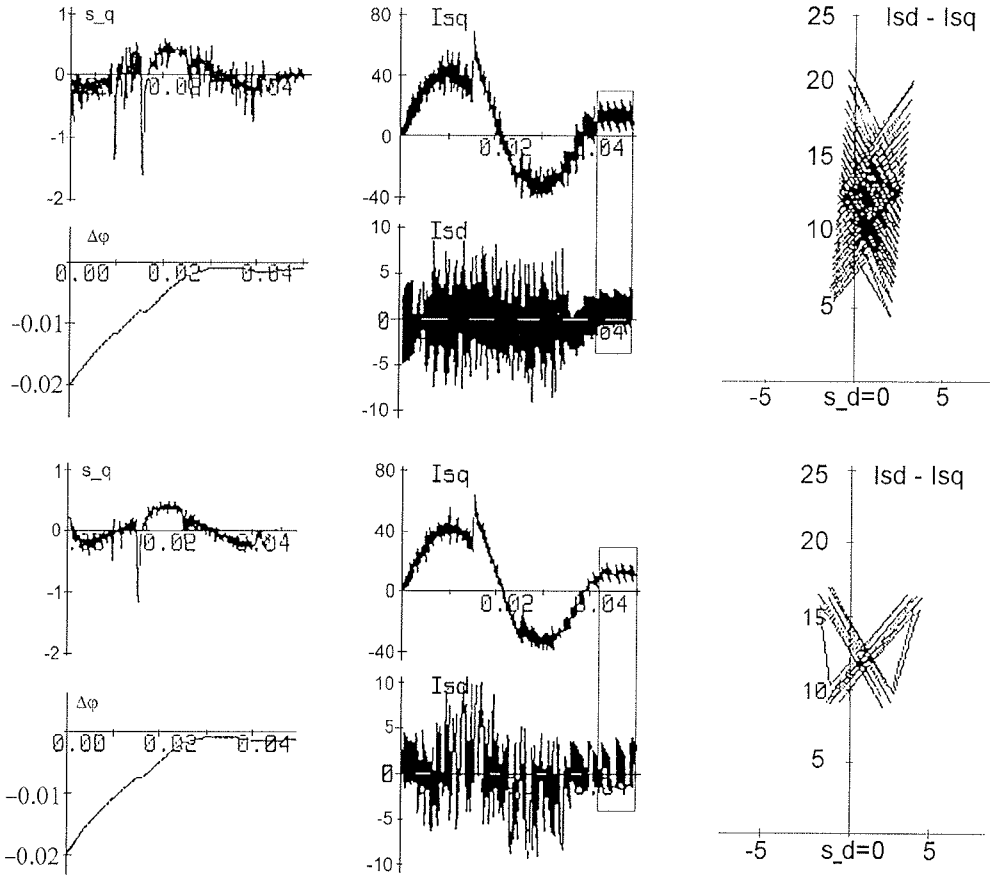

Fig. 7. Tracking the disturbed task simulation results for SCC (top), and BLSC (bottom). $T_s = 25\,\mu s$, [A] $\Delta\varphi = \varphi^{REF} - \varphi$ [rad], s_d and s_q are s_d and s_q respectively. Trajectories of i_S are at $\varphi = 4,75$ [rad] at the indicated 5 ms intervals.

ration of FOC and the use of feedforwarded $\dot{\rho}$ Using these measures, more current ripples are directed into magnetization (where it is well dampened by rotor lag) than to torque generation.

Preassigned switching order also enables the employment of zero-voltage vectors. Their use reduces deviation of the **s** local average at S_0, thus reducing the chattering, as well as the total inverter switching frequency. With feedforwarding $\dot{\rho}$ becomes possible the compensation for deviation of the local average s_q at active voltage vectors and also it enables extension of $\dot{\rho}$ with nominal rotor field.

Finally, it is worth mentioning that despite to all refinements, current control still has a relatively simple structure, which can be efficiently implemented in digital signal processors. The proposed VSC with voltage mapping is also implementable in all symmetric 3-phase motor types.

Biblography

/1/ F. Hashimoto, H. Yamamoto, S. Yaganisava: Brushless servomotor control using variable structure approach. *IEEE tarns. IA.*, vol IA24, pp 160–170, 1988

/2/ Ž. Čučej, P. Cafuta: Current controllrd pulse-width modulations for output voltage of inverters feeding AC motors, part 3: sliding mode control. *Elektrotechnical review*, ISSN 0013-5852 Vol. 66, No. 1, pp. 58–66, 1999

/3/ Ž. Čučej, P. Cafuta: *Optimization of the supply voltage pattern in the sliding mode controlled induction motor drive.* ISIE'99 Bled Slovenia, Proceeding Vol. 1, pp. 7–13, 1999

/4/ P. Cafuta: *Determination of inverter switching by intermodulation: sliding mode controlled IM drive*. Invited presentation on University Johanes Kepler, Linz, Avstrija, 1999

/5/ W.C. Su, S.V. Drakunov, Ü. Özzgüner: An $O(T^2)$ Bounary Layer in Sliding Mode for Sampled data System. *IEEE Trans. on Automatic Control*, Vol. 45. No. 3. pp. 482–485, 2000

/6/ N. Šabanović-Behlilović, A. Šabanović, T. Ninomiya, *PWM in three-phase switching conwerters - sliding mode soluton.* Conference PESC'94, Taipeh, Proceedings, pp. 560–565, 1994.

/7/ J. Holtz, S. Stadtfeld, Pulsewidth modulation for electric power conversion. *Proceedings of IEEE*, Vol. 82, No. 8. pp. 1194–1214, 1994.

/8/ W. Leonhard, 30 years space vectors, 20 years field orientation, 10 years digital signal processing with controled AC drives. *EPE Journal*, Vol. 1 and Vol. 2, 1991.

/9/ V.I. Utkin, Sliding mode control design principle and applications to electric drives. *IEEE Trans. on Ind. Electronics*, Vol. 40, No. 1, pp. 23–35, 1993.

/10/ W. Gao, J. C. Hung, Variable structure control of nonlinear systems: a new approach. *IEEE Trans. on Ind. App.*, Vol. 40, No. 1, pp. 45–55, 1993.

/11/ C. Rossi, A. Tonielli, Robust current controller for three-phase inverter using finite-state automaton. *IEEE Trans. on Ind. Electronics*, Vol. 42, No. 2, pp. 169–178, 1995.

Appendices

A. Kinematic tracking

The drive dynamics is described with

$$J\dot{\omega} = T_e - T_L, \tag{20}$$

where $\omega = \dot{\varphi}$ is rotor angular velocity and *J* is drive inertia constant or variable as load torque T_L. By tracking, kinematics' variables $\dot{\varphi}^{REF}$ (speed) and φ^{REF} (rotor position) are prescribed functions. IM delivers electrical torque decoupled from magnetization by FOC:

$$T_e = \frac{2}{3}\frac{P}{2}\frac{L_m}{L_S L_R} i_{mR} i_{Sq} = k_m i_{Sq}, \tag{21}$$

where *P* is number of the machine poles, L_m, L_R and L_S are mutual, rotor and stator inductances respectively, i_{mR} present rotor magnetization current /8/. The rotor field angle:

$$\rho = \int \dot{\rho}\, dt = \int \left\{ P\omega + \frac{2}{P}\frac{i_{Sq}}{i_{mR}} \right\} dt \tag{22}$$

is determined according to the rotor lag τ_R. If an error of position, angular speed and acceleration forms a linear combination, then the control task can be determined as:

$$c_1 e + c_2 \dot{e} + \ddot{e} = 0 \tag{23}$$

where $e = \varphi - \varphi^{REF}$, $\dot{e} = \dot{\varphi} - \dot{\varphi}^{REF}$ and $\ddot{e} = \ddot{\varphi} - \ddot{\varphi}^{REF}$ are the position, angular speed and acceleration error respectively, and c_1 and c_2 are positive constants. From (23) follows

$$\ddot{e} = \ddot{\varphi}^{REF} - \ddot{\varphi} = c_1 e - c_2 \dot{e} \tag{24}$$

and considering (20) and (4) the current reference is given as:

$$i_{Sq}^{REF} = \left(c_1 e + c_2 \dot{e} + \ddot{\varphi}\right)\frac{J}{k_m} - \frac{\hat{T}_L}{k_m} \tag{25}$$

where $\hat{T}_L$ is estimated value of T_L. From (25) follows, that e, $\dot{e}$, and $\ddot{e}$ are projected on a current error plane as current error in *q*-axis direction of FOC. Maximal ratio between them and $\| s \|_2$ is bounded by the selection of constants c_1 and c_2 regarding stability and robustness of the controlled system.

B. Rotor magnetization control

If the rotor magnetization is represented by the rotor magnetization current i_{mR} /8/, then the magnetization model is determined by:

$$\tau_R \, pi_{mR} + i_{mR} = i_{Sd} . \tag{26}$$

Magnetization due to FOC is a slow process, in relation to torque production; thus, the offset caused by e_d can be minimized by a suitably designed magnetization current control. Using the same reasoning as kinematics tracking, the magnetization current error is expressed as

$$e_m = i_{mR}^{REF} - \hat{i}_{mR} \tag{27}$$

where $\hat{i}_{mR}$ is an estimate. The current reference is:

$$i_{Sd}^{REF} = c_3 \varepsilon_m + \left(pi_{mR}^{REF} - \frac{\hat{i}_{mR}}{\tau_R} \right) \frac{L_m}{R_R} . \tag{28}$$

C. Modified induction motor model

After calculating $i_{S\Diamond}$ from (4), the equation (3) rewritten in the error form /11/ becomes:

$$u_{k\Diamond}(\rho) = R_S i_{S\Diamond}^{REF} - R_S s_\Diamond + L_{S\sigma} \, pi_{S\Diamond}^{REF} - L_{S\sigma} \dot{s}_\Diamond + e_\Diamond \tag{29}$$

and when rearranged is

$$L_{S\sigma} \, \dot{s}_\Diamond = u_{k\Diamond}(\rho) - R_S s_\Diamond - d_\Diamond . \tag{30}$$

The term

$$d_\Diamond = L_{S\sigma} \, pi_{S\Diamond}^{REF} - R_S i_{S\Diamond}^{REF} - e_\Diamond \tag{31}$$

collects all the disturbances (exogenous and endogenous) acting on the system. It is known that the current tracking problem (3) is equivalent to the stabilization of (30). Because $L_{S\sigma}$ and R_S are semipositive values, the term $-R_S s_\Diamond$ is always stabilizing, i.e. any feedback that stabilized (31) with $R_S = 0$ also stabilizes it with $R_S > 0$. Moreover, the stator windings resistance in IM is usually low, and the term $-R_S s_\Diamond$ can be neglected. Furthermore, considering that i_{Sq}^{REF} during the sampling interval is constant, its derivation is zero. From (31) it follows that $d_\Diamond = e_\Diamond$. Hence, the simplified model

$$L_{S\sigma} s_\Diamond(\rho) = u_{k\Diamond}(\rho) - e_\Diamond \tag{32}$$

is assumed in presented design.

D. Stability analysis

For attraction domain A_0 the reaching condition is derived by second Lyapunov method /9/ from quadratic form $\frac{1}{2} ss^T$, $V \geq 0$ as:

$$\dot{V} = \dot{s}_d s_d + \dot{s}_q s_q \leq 0 . \tag{33}$$

Considering simplified IM model (2) at constant rotor field, where $pi_{mR} = 0$ and consequently $e_{id} = 0$, condition (33) can be written as:

$$\dot{V} = \frac{s_d}{L_{S\sigma}} \left[u_{kd}(\rho) - e_{dq} \right] + \frac{s_q}{L_{S\sigma}} \left[u_{kq}(\rho) - e_{iq} - e_{dq} \right] \leq 0 \tag{34}$$

In the case of selected zero voltage vectors (34) becomes:

$$\dot{V} = \frac{s_d}{L_{S\sigma}} \left[-e_{dq} \right] - \frac{s_q}{L_{S\sigma}} \left[e_{iq} + e_{dq} \right] \leq 0 \tag{35}$$

and it is also evident that it is negative as long as $\dot{\rho} \neq 0$ and the condition (19) for selecting of zero voltage vectors is fulfilled.

In the case of $\dot{\rho} = 0$, (34) is equal to zero, meaning that the system is at a standstill. But there is an assumption for neglecting the influence of R_S for simplified IM model is not valid anymore, consequently full IM model had to be considered in (33). Assuming selection of zero voltage and that during sample interval i_S^{REF} is constant, (35) becomes:

$$\dot{V} = -\frac{s_d}{L_{S\sigma}} R_S i_{Sd} - \frac{s_q}{L_{S\sigma}} R_S i_{Sq} \tag{36}$$

which is negative until the condition (10) is satisfied, since according to (19) signs of s_q and e_q are reciprocal. Those facts can serve as proof of the following theorem:

Theorem: Zero voltage maintains sliding along switching lines, or limit cycle around the error plane origin, if and only if their use satisfies the conditions of (10) and (19).

Žarko Čučej,
Peter Cafuta, and
Rajko Svečko
University of Maribor, Slovenia
e-mail: zarko.cucej@uni-mb.s

Prispelo (Arrived): 24.03.2001 *Sprejeto (Accepted): 01.06.2001*